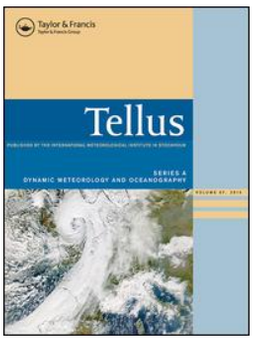

Tellus A: Dynamic Meteorology and Oceanography

ISSN: (Print) 1600-0870 (Online) Journal homepage: https://www.tandfonline.com/loi/zela20

Internal variability in a 1000-yr control simulation with the coupled climate model ECHO-G — I. Near-surface temperature, precipitation and mean sea level pressure

Seung-Ki Min, Stephanie Legutke, Andreas Hense & Won-Tae Kwon

To cite this article: Seung-Ki Min, Stephanie Legutke, Andreas Hense & Won-Tae Kwon (2005) Internal variability in a 1000-yr control simulation with the coupled climate model ECHO-G — I. Near-surface temperature, precipitation and mean sea level pressure, Tellus A: Dynamic Meteorology and Oceanography, 57:4, 605-621, DOI: 10.3402/tellusa.v57i4.14712

To link to this article: https://doi.org/10.3402/tellusa.v57i4.14712

Published online: 15 Dec 2016.

Tellus (2005), 57A, 605–621
Printed in Singapore. All rights reserved

TELLUS

Internal variability in a 1000-yr control simulation with the coupled climate model ECHO-G – I. Near-surface temperature, precipitation and mean sea level pressure

By SEUNG-KI MIN[1]*, STEPHANIE LEGUTKE[2], ANDREAS HENSE[1] and WON-TAE KWON[3], [1]*Meteorological Institute, University of Bonn, Auf dem Hügel 20, 53115 Bonn, Germany;* [2]*Max Planck Institute for Meteorology, Bundesstrasse 53, 20146 Hamburg, Germany;* [3]*Meteorological Research Institute, 460-18 Sindaebang-dong, Dongjak-gu, Seoul 156-720, Korea*

(Manuscript received 30 July 2004; in final form 20 December 2004)

ABSTRACT

The internal variability in a 1000-yr control simulation with the coupled atmosphere–ocean global climate model ECHO-G is analysed using near-surface temperature, precipitation and mean sea level pressure variables, and is compared with observations and other coupled climate model simulations. ECHO-G requires annual mean flux adjustments for heat and freshwater in order to simulate no significant climate drift for 1000 yr, but no flux adjustments for momentum. The ECHO-G control run captures well most aspects of the observed seasonal and annual climatology and of the interannual to decadal variability of the three variables. Model biases are very close to those in ECHAM4 (atmospheric component of ECHO-G) stand-alone integrations with prescribed observed sea surface temperature. A trend comparison between observed and modelled near-surface temperatures shows that the observed near-surface global warming is larger than internal variability produced by ECHO-G, supporting previous studies. The simulated global mean near-surface temperatures, however, show a 2-yr spectral peak which is linked with a strong biennial bias of energy in the El Niño Southern Oscillation signal. Consequently, the interannual variability (3–9 yr) is underestimated.

1. Introduction

Knowledge of internal climate variability is not only necessary for climate change detection and attribution studies, but also fundamental for climate change projections and model evaluations (e.g. Collins et al., 2001). Instrumental observational records are known to be insufficient for a proper estimation of internal climate variability on long time-scales due to their short temporal and spatial coverage. Also, they are contaminated by unknown external forcing, e.g. volcanic eruptions, changes in solar output as well as the anthropogenic emission of greenhouse gases, sulphate aerosols, and ozone depleting gases (Stouffer et al., 2000). Although proxy climate data, such as tree rings, historical documents and sediments, provide important information about the past climate on long time-scales, they are too sparse spatially to give accurate global signals (e.g. Barnett et al., 1999). As a surrogate for natural climate variability, atmosphere–ocean coupled general circulation models (AOGCMs) have been used widely for climate studies.

*Corresponding author.
e-mail: skmin@uni-bonn.de

Studies of climate variability on annual to decadal time-scales require simulation lengths of O(1000a). There have been several control integrations of more than 1000 yr (i.e. with fixed external forcing; see Table 1): CCSM2.0, CGCM1, CSIRO_Mk2, DOE PCM, ECHAM1/LSG, ECHAM3/LSG, GFDL_R15_a, GFDL_R30, HadCM2 and HadCM3 (in alphabetical order), which were performed at the National Center for Atmospheric Research (NCAR), the Canadian Centre for Climate Modelling and Analysis (CCCma), the Commonwealth Scientific and Industrial Research Organization (CSIRO), the German Climate Computer Centre (Deutsches Klimarechenzentrum, DKRZ), the Geophysical Fluid Dynamics Laboratory (GFDL), and the United Kingdom Meteorological Office (UKMO), respectively. All model runs except for CCSM2.0, HadCM3 and DOE PCM use flux adjustments (Table 1). The climatology and variability in the control runs of each model have been analysed and compared with observations (see the references in Table 1), and intercomparisons between model runs have been carried out in terms of internal variability of near-surface temperature (Stouffer et al., 2000; Braganza et al., 2002) and various atmospheric and oceanic variables (von Storch et al., 2000, 2001; Monahan and Dai, 2004).

Table 1. List of millennium control integrations of AOGCMs (alphabetical order) and analysed variables for the internal climate variability

Model (Institution)	Total (analysed) integration length (yr)	Analysed variables[a]	Resolutions (atmosphere/ ocean)[b]	Flux adjustments[c]	References
CCSM2.0 (NCAR)	1000	ENSO, NAO, THC	T42 (2.8× 2.8) L26/ 0.54# × 1.125 40L	–	Kiehl and Gent (2004), Holland (2003), Hu et al. (2004)
CGCM1 (CCCma)	1000 (200)	T2m, PCP, MSLP, ENSO, THC, PDO	T32 (3.8×3.8) L10 /1.856×1.875 L29	H, W	Flato et al. (2000), Yu and Boer (2004)
CSIRO Mk2 (CSIRO)	1000	T2m[4], ENSO	R21 (3.2×5.6) L9/3.2×5.6 L21	M, H, W	Hirst et al. (2000), Vimont et al. (2002), Hunt and Elliott (2003)
DOE PCM (NCAR)	1000 (300)	T2m, ENSO[5], THC	T42 (2.8×2.8) L18/ 0.67#×0.67 L32	–	Washington et al. (2000)
ECHAM1/LSG (DKRZ)	1260	T2m, THC[2,3], V200[3], V500[3], V850[3]	T21 (5.6×5.6) L19/4.0×4.0 L11	M, H, W	von Storch et al. (1997)
ECHAM3/LSG (DKRZ)	1000	T2m[1], SST[3], THC[2,3]	T21 (5.6×5.6) L19/4.0×4.0 L11	M, H, W	Voss et al. (1998), Timmermann et al. (1999)
ECHO-G (M&D MPIfM)	1000	T2m, ACW, ENSO	T30 (3.75×3.75) L19/2.8#×2.8 L20	H*, W*	Zorita et al. (2003), Marsland et al. (2003), Rodgers et al. (2004)
GFDL_R15_a (GFDL)	1000	T2m[1], SST, THC[2,3]	R15 (4.5×7.5) L9/4.5×3.7 L12	H, W	Manabe and Stouffer (1996)
GFDL_R30_b,c (GFDL)	1000, 900	T2m, ENSO[5], AO, THC	R30 (2.25×3.75) L14/2.25×1.875 L18	H, W	Delworth et al. (2002)
HadCM2 (UKMO)	1700	T2m[1,4], ZMT, ENSO, NAO, THC[2,3]	2.5×3.75 L19/2.5×3.75 L20	H, W	Tett et al. (1997), Osborn et al. (1999), Gillett et al. (2000), Collins (2000)
HadCM3 (UKMO)	1000	T2m[4], ZMT, ENSO[5], NAO	2.5×3.75 L19/1.25×1.25 L20	–	Collins et al. (2001)

[a]The abbreviations used are as follows: Antarctic Circumpolar Wave (ACW); Arctic Oscillation (AO); Pacific Decadal Oscillation (PDO); thermohaline circulation (THC); V'mmm' ('mmm'-hPa wind); zonal mean temperature (ZMT). The numbers 1–5 indicate the analyses carried out by Stouffer et al. (2000), von Storch et al. (2000, 2001), Braganza et al. (2002), and Monahan and Dai (2004), respectively.

[b]Latitude × longitude with a spectral truncation. The symbol (#) depicts the equatorial latitudinal refinement. Vertical resolution is expressed as 'L' + number of vertical levels.

[c]M denotes momentum flux, H denotes heat flux, and W denotes freshwater flux. An asterisk (*) indicates annual mean flux adjustment only.

Recently, a 1000-yr control simulation (CTL) has been carried out using ECHO-G, an AOGCM developed by the Model and Data group (M&D) at the Max Planck Institute for Meteorology (MPIfM). The atmospheric component of ECHO-G is ECHAM4 (Roeckner et al., 1996) and the oceanic component is HOPE-G (Legutke and Maier-Reimer, 1999). The objective of this paper is to describe the climatology and internal variability of an ECHO-G control run and to validate them by comparison with observations for surface variables such as temperature, precipitation and mean sea level pressure (MSLP). In a companion paper (Min et al., 2005, hereafter Paper II), the simulation skills for two dominant phenomena of natural climate variability, the El Niño Southern Oscillation (ENSO) and the North Atlantic Oscillation (NAO), are evaluated. This paper will be a background for future studies of climate change detection and projections using ECHO-G ensemble simulations with Intergovernmental Panel on Climate Change (IPCC) scenarios.

The ECHO-G model, the integration method of the CTL and the observational data sets used for model validation are described in the next section. The climatology and internal variability of the surface variables in ECHO-G CTL are compared with observations in Section 3. A summary of analysis results is given in the last section.

2. Model and observations

2.1. Model description

ECHO-G consists of two component models: the atmospheric component ECHAM4 containing a land surface scheme and the oceanic component HOPE-G with an embedded sea-ice model. ECHAM4 is the fourth generation version of the Hamburg atmospheric general circulation model (AGCM), which was modified from the European Centre for Medium-Range Weather Forecasts

(ECMWF) AGCM for use in long-term climate simulations. A general model description and validation of the present-day climate simulations with ECHAM4 are given by Roeckner et al. (1996). The standard ECHAM4 has been modified for ECHO-G such that the heat, freshwater and momentum fluxes are calculated separately for the ice-covered and the ice-free part of each ocean grid cell, following Grötzner et al. (1996). To close the freshwater and heat budgets, a scheme for continental and river runoff and ice discharge from continental ice sheets has been implemented (Legutke and Voss, 1999). The formulation of the ice discharge, which includes the release of latent heat of fusion associated with a mass discharge from the continental ice sheets of Greenland and Antarctica to close the heat budget in the coupled system, was shown to greatly improve the bottom water formation near the Antarctic coast (Legutke, 2000).

It has been shown that ECHAM4 performs well on a T30 grid relative to the standard version on a T42 grid (triangular truncation 30/42; Stendel and Roeckner, 1998). In addition, HOPE-G showed overall similar performance when forced by T30 ECHAM4 model data or T42 data (Legutke et al., 1996). Therefore, the T30 grid version ($\sim$3.75°) of ECHAM4 is used for the 1000-yr control integration in order to improve computational efficiency. The vertical resolution of ECHAM4 is defined by 19 hybrid sigma-pressure levels with the highest level at 10 hPa.

The ocean model HOPE-G is the global version of the Hamburg Ocean Primitive Equation (HOPE) model and includes a dynamic–thermodynamic sea-ice model with a viscous–plastic rheology (Hibler, 1979) and snow cover. A Gaussian T42 grid ($\sim$2.8°) is used with a gradual meridional refinement reaching 0.5° in the tropical oceans between 10°S and 10°N. The vertical resolution is given by 20 horizontal levels with eight levels within the top 200 m from the ocean surface. HOPE-G has been little changed from Wolff et al. (1997) except for the thermodynamic ice growth, which is computed from the fluxes obtained from the atmospheric model rather than from heat-balance equations based on bulk formulae. The climatology of HOPE-G, forced by atmospheric fluxes obtained from an experiment with ECHAM4 using Atmospheric Model Intercomparison Project (AMIP) sea surface temperature (SST), is described in detail by Legutke and Maier-Reimer (1999).

ECHAM4 and HOPE-G are coupled by the OASIS software (Valcke et al., 2000). They exchange 10 daily mean atmospheric fluxes (zonal and meridional momentum flux over water and over ice, solid freshwater flux over ice, liquid freshwater flux, downwelling solar heat flux, net heat flux over water, conductive and residual heat flux over ice) and four surface conditions (SST, sea ice concentration and thickness, snow depth) once a day. The model time-steps are 30 min for ECHAM4 and 12 h for HOPE-G. A more detailed description of the coupling techniques of ECHO-G can be found in Legutke and Voss (1999). ECHO-G is a descendant of the coupled GCM ECHO-1 (Latif and Barnett, 1994, 1996; Latif et al., 1994; Schneider et al., 1996; Grötzner et al., 1998) and ECHO-2 (Frey et al., 1997; Pierce et al., 2000; Venzke et al., 2000). The ancestor models (ECHO-1 and ECHO-2) did not include a sea-ice component but relaxed SSTs to observed climatological values poleward of 60°.

2.2. *Control simulation*

After a stand-alone integration of 18 yr of the atmosphere and 2034 yr of the ocean, an initial coupled integration of 155 yr was performed. In this initial spin-up, SST and sea surface salinity (SSS) were relaxed to seasonal climatological values. However, no salinity relaxation was applied in the AMIP climatological sea-ice regions to avoid distortion of the upper-ocean salinity changes related to ice production. Annual mean heat and freshwater fluxes, as diagnosed from the relaxation terms during the last 100 yr of the coupled spin-up phase, are used as flux adjustments for the CTL. Both flux fields are normalized to vanish globally. No momentum flux adjustments are applied. This flux-adjustment method has the merit of leaving the seasonal cycle and the wind stress determined by model, as well as freshwater fluxes in sea-ice regions related to the ice melting and freezing processes. Present-day concentrations are used for the three main greenhouse gases, CO_2, CH_4 and N_2O (353 ppmv, 1720 ppbv and 310 ppbv, respectively).

The ECHO-G CTL data have been used for some recent climate variability studies. Baquero-Bernal et al. (2002) investigated the dependence of the Indian Dipole mode on the ENSO, comparing the first 100 yr from the control run with a 100-yr simulation in which the ENSO variability was suppressed by relaxation to climatological mean model SST. Zorita et al. (2003) assessed an uncertainty in a paleoclimate reconstruction method. Marsland et al. (2003) examined the variability of the Antarctic Circumpolar Wave and Rodgers et al. (2004) analysed decadal modulations of ENSO.

2.3. *Observation-based data*

The observational data used in this study are listed in Table 2 for each variable with source, resolution, analysis period and key references. Near-surface temperature (T2m), precipitation (PCP) and MSLP are regarded as 'basic' surface variables. T2m is obtained from the Climate Research Unit (CRU). The Climate Prediction Center (CPC) Merged Analysis Precipitation (CMAP) is used as PCP observations. The National Centers for Environmental Prediction (NCEP) and the NCAR provided reanalysis of the MSLP. T2m, PCP and MSLP from the model simulations and observations are interpolated on to a common 5° × 5° grid before analysis. The global mean is defined as the area-weighted average between 85°S and 85°N of the interpolated data, excluding the poles where the interpolated data are not defined in the simulations. There is little change in the variance of T2m after interpolation, e.g. +0.62% for the simulated global mean annual values, but considerable changes in the variances

Table 2. Observational data for each analysed variable

Variable (abbreviation, unit)	Source	Resolution	Analysis period	References
Near-surface temperature (T2m, °C)	HadCRUT2	5° × 5°	1856–2001	Jones and Moberg (2003) Rayner et al. (2003)
Sea surface temperature (SST, °C)	GISST2.2	1° × 1°	1903–1994	Rayner et al. (1996)
Precipitation (PCP, mm d^{-1})	CMAP	2.5° × 2.5°	1979–1999	Xie and Arkin (1997)
Mean sea level pressure (MSLP, hPa)	NCEP/NCAR reanalysis	2.5° × 2.5°	1958–2001	Kistler et al. (2001)

of PCP (+4.02%) and MSLP (−5.31%). To consider possible changes of the variances caused by using different horizontal resolutions, we compare simulated and observed variances on the common 5° × 5° grid.

The observations of HadCRUT2 have space- and time-varying missing data points, while the model has no missing data. Also, the observations represent a shorter time period than the 1000 yr of model control data. Therefore, the model data on grid points where observational data are missing are treated as missing and are referred to as 'masked' model data, and the 1000 yr of ECHO-G CTL are divided into subperiods with the same length as the observational period.

3. Variability of surface variables

The overall performance of ECHO-G is described now for the basic surface variables, i.e. T2m (including SST), PCP and MSLP. After evaluating model-simulated long-term climate including global and zonal mean patterns for the variables, the spatial patterns of interannual variability and the power spectra are compared with the observations.

3.1. Near-surface temperature

The global mean T2m retains a seasonal cycle due to the hemispheric differences of land–sea distribution. The annual

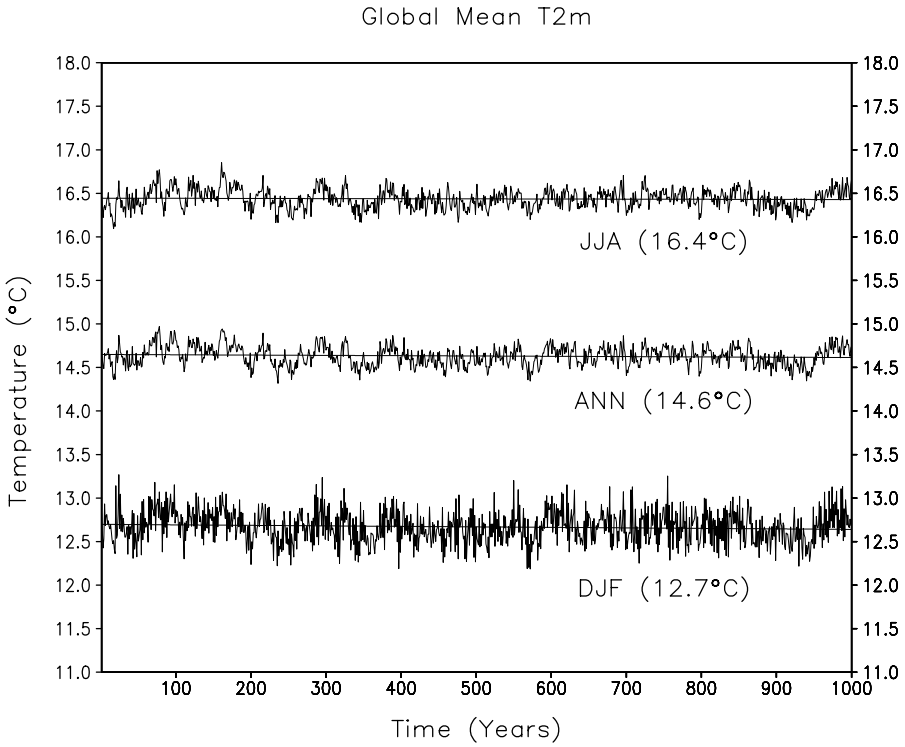

Fig. 1. Annual (ANN) and seasonal (DJF, JJA) mean time series of global mean near-surface temperature from the ECHO-G CTL. Values in parentheses are 1000-yr mean, and solid lines are linear trends. Observational values estimated from HadCRUT2 (1961–1990; Jones et al. (1999)) are 14.1, 12.4 and 15.9°C for ANN, DJF and JJA, respectively.

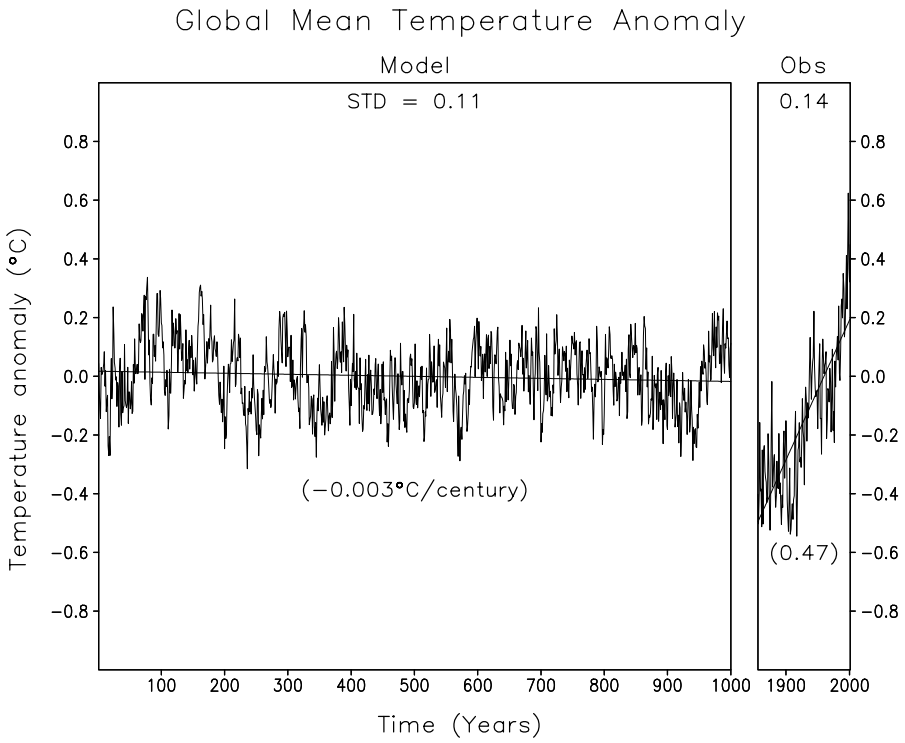

Fig. 2. Time series of global annual mean near-surface temperature anomalies from ECHO-G CTL and HadCRUT2 observations (1856–2001). Solid lines are linear trends. Their values are given in parentheses (°C per century).

(ANN), June–August (JJA) and December–February (DJF) mean time series of global mean T2m are shown in Fig. 1. Corresponding observed values (estimated from the 1961–1990 climate of HadCRUT2; Jones et al., 1999) are 14.1°C, 15.9°C and 12.4°C, respectively. Thus, the ECHO-G model climate is somewhat warmer (0.3–0.5°C) than that observed. No significant drift in surface temperature occurs in the ECHO-G climate (−0.003°C per century). In contrast, observed temperatures show a positive trend of 0.47°C per century (see Fig. 2). The standard deviation (STD) of linearly detrended global mean T2m of ECHO-G CTL is 0.11°C, which is smaller than the STD of the detrended observed T2m, which is 0.14°C. Compared to other model results, it is close to those of HadCM2 and HadCM3 (0.13°C and 0.12°C, respectively; Collins et al., 2001) and larger than that of ECHAM3/LSG (0.07°C).

The power spectrum of global mean T2m is compared with the observed following the method used by Collins et al. (2001). The Blackman–Tukey method (Blackman and Tukey, 1958) is used for performing spectral analysis with a Hamming window. A maximum lag of 25 yr is applied. The monthly global temperature anomaly time series from the 1000-yr control run is divided into 10 100-yr periods and the space- and time-varying missing-data information from the observational data (HadCRUT2, 1901–2000) are used to mask the model data. The power spectra of area-weighted global mean temperatures are calculated, after the linear trends have been removed, for each 100-yr subsection of model data and for the observations.

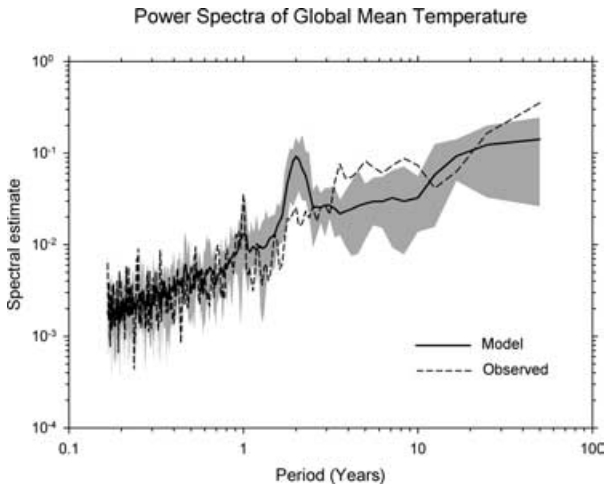

Fig. 3. Power spectra of the global mean T2m from the ECHO-G CTL (solid line) and HadCRUT2 observations (dashed line, 1901–2000). The shading indicates the maximum and minimum spectral estimates from 10 100-yr sections of the ECHO-G CTL, and the solid line is an average of the 10 power spectra.

Figure 3 shows the power spectra of the global mean temperatures. While the power spectrum of the observation has no significant peak against an AR(1) process (Hasselmann, 1976), a statistically significant 2-yr peak appears in the model data. According to Gillett et al. (2000) the model data and the observations are

Table 3. Trends of global temperature anomaly in the HadCRUT2 observation and corresponding trend occurrences greater than the observed trends in the ECHO-G CTL. Values in parentheses denote the results from 'masked' ECHO-G CTL

Observation period (yr)	Trend length (yr)	Observed trend (°C per century)	Model trend occurrence			
			Occurrence		Relative occurrence (%)	
1992–2001	10	3.2	23	(18)	2.3	(1.8)
1987–2001	15	1.6	73	(46)	7.4	(4.7)
1982–2001	20	2.0	0	(0)	0.0	(0.0)
1977–2001	25	1.8	0	(0)	0.0	(0.0)
1972–2001	30	1.9	0	(0)	0.0	(0.0)
1962–2001	40	1.4	0	(0)	0.0	(0.0)
1952–2001	50	1.0	0	(0)	0.0	(0.0)
1902–2001	100	0.7	0	(0)	0.0	(0.0)
1856–2001	146	0.5	0	(0)	0.0	(0.0)

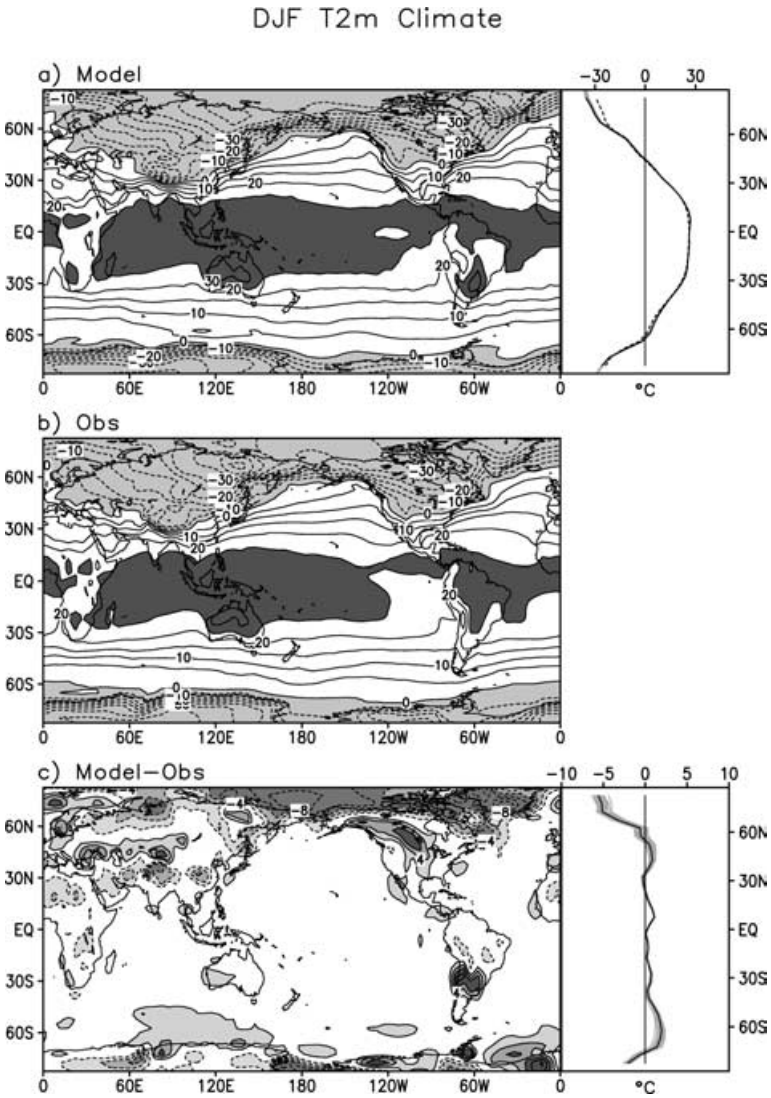

Fig. 4. T2m climate in DJF for model (a), observations (b), and model minus observation (c). Contour intervals are 5°C in (a) and (b) and 2°C in (c). The zero line is omitted in (c). Zonal means for the model (solid line) and the observation (dashed line) are plotted together in the upper-right panel. The zonal mean of model biases is presented in the lower-right panel. Light solid lines in the zonal mean plots represent the results from 33 30-yr subsections of ECHO-G CTL.

significantly different at the 93% level (ln 2/10 independent subsections) in the periods of around 2 and 3–9 yr. The model has more energy in the 2-yr period and less power in the period of 3–9 yr than the observations. These spectral characteristics of the modelled T2m are related to a strong 2-yr periodicity in the ENSO variability (see Paper II). Observed spectral power is outside the simulated range at the longest period (50 yr), which might be due to the external forcing even allowing for the detrending procedure described above.

Considering that the decadal variability of global mean T2m in ECHO-G CTL compares well with the observations (Fig. 3), we investigated the probability of occurrence of trends greater than the observed trends following Collins et al. (2001); see Table 3. Numbers of trend occurrences in the ECHO-G CTL are obtained from moving windows for specified periods. The maximum observed trend of 3.2°C per century appears in the recent 10-yr period (1992–2001). There is a 2.3% chance of finding a larger trend in ECHO-G CTL. For periods of 20 yr and longer, there is no occurrence in the model of trends larger than the maximum observed value, which is consistent with the HadCM3 results of Collins et al. (2001). This result holds for the 'masked' and 'unmasked' model data (see the values in parentheses in Table 3).

Figures 4 and 5 show the geographical patterns of DJF and JJA T2m, respectively, of the model and observations, as well as their zonal mean difference. The simulated T2m, which most AOGCMs are known to simulate well (e.g. Lambert and Boer, 2001), is very similar to the observations, both for the geographical and zonal mean patterns, except that the zonal mean temperature distributions display cold biases in the Northern Hemisphere (NH) high latitudes, while warm biases appear in the Southern Ocean. Note that the T2m are strongly dependent on the presence of an ice cover in ocean cells. The Arctic domain and the Himalayan mountain ranges are dominated by cold biases. The Arctic cold bias in JJA is opposite to the warm bias in the

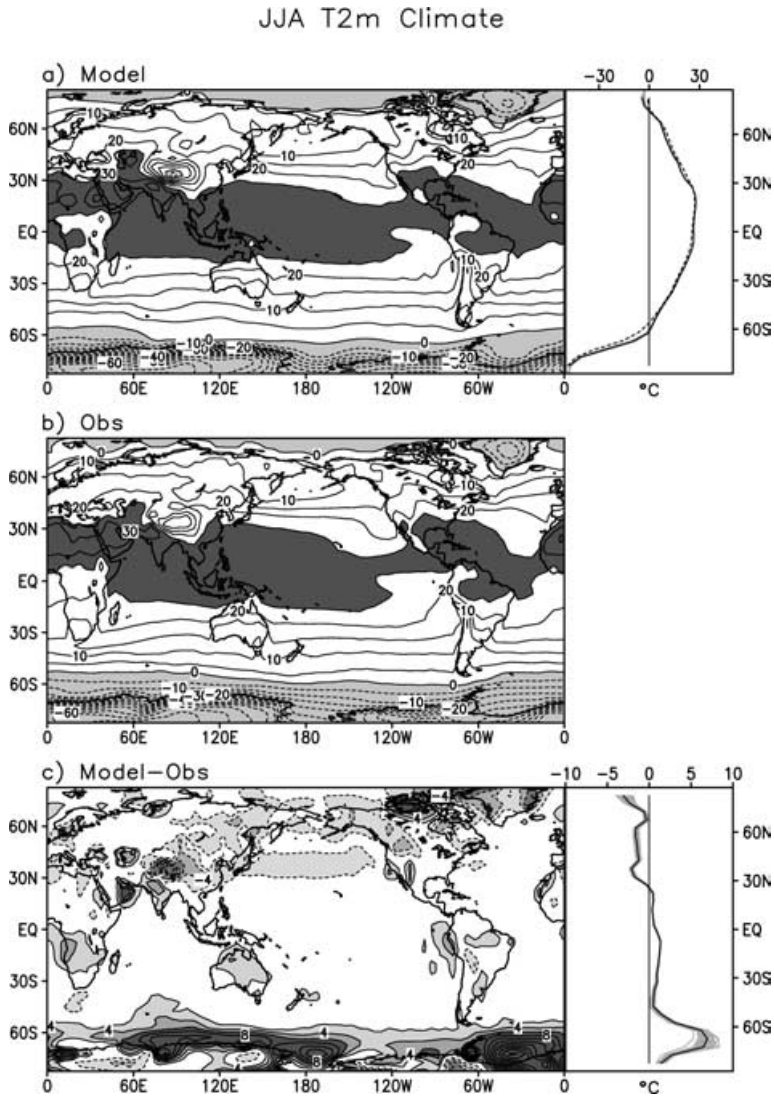

Fig. 5. Same as Fig. 4 but for JJA T2m.

ECHAM4 simulations with prescribed observed SSTs (Roeckner et al., 1996). Warm biases are significant over mid-latitude continental areas of both hemispheres during DJF, while cold biases appear in NH mid-latitude continents in JJA. The JJA cold bias on the Asian continent indicates a decreased land–sea contrast and may account partly for the weak Asian summer monsoon in the model climate shown in Fig. 10c (see also Hu et al., 2000).

To assess the model skill at simulating local temperature variability, the model STD is calculated by averaging 10 STD patterns of 'masked' 100-yr periods. The result is compared with the STD of the 100-yr (1901–2000) HadCRUT2 observations. To remove climate signals from external forcing in the simplest way, linear trends are removed locally before calculating STDs of the model and observations (Stouffer et al., 2000). More than 10 months for annual mean and more than 30 yr for

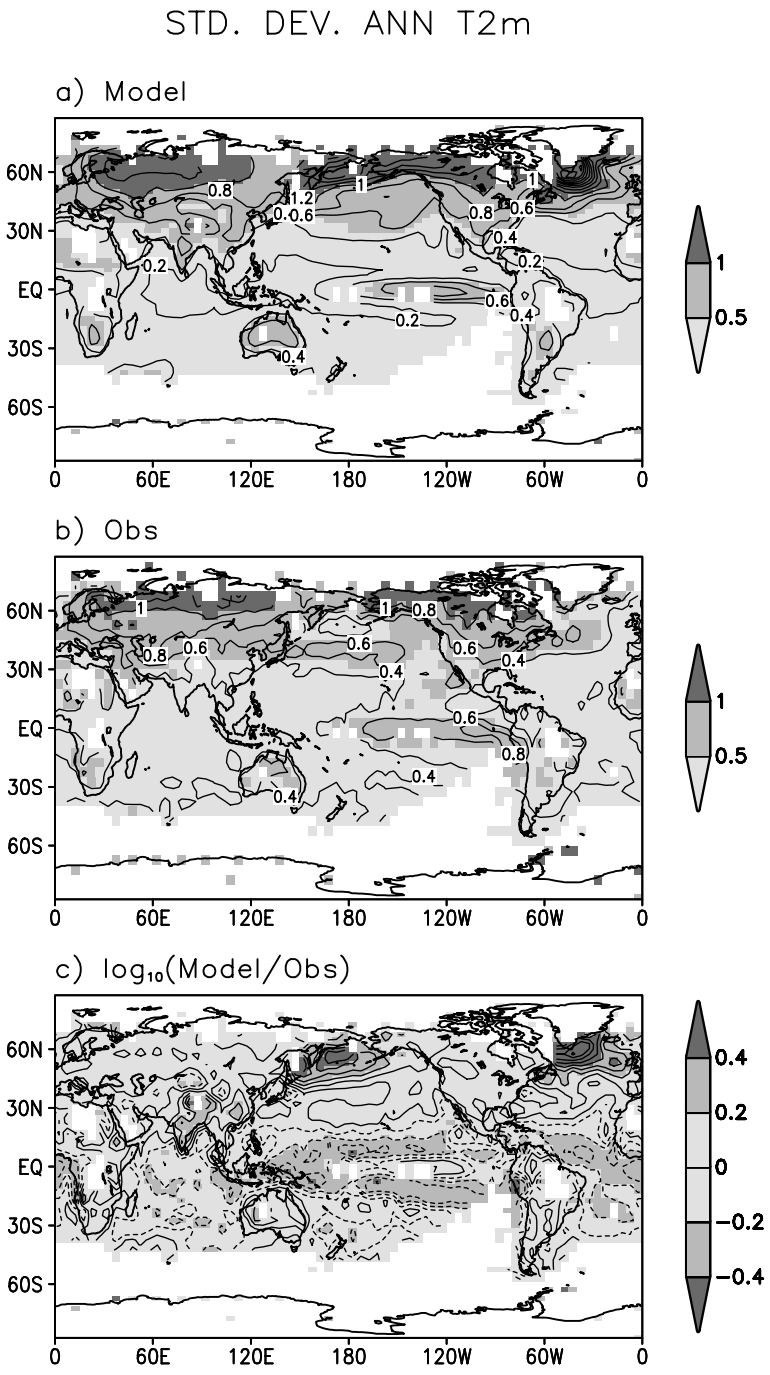

Fig. 6. Spatial distribution of the STD of annual mean T2m from ECHO-G CTL (a) and observations (b) and the logarithm of their ratio (c). Contour intervals are 0.2°C in (a) and (b) and 0.1 in (c). Solid lines are for positive values and dotted lines for negative values in (c).

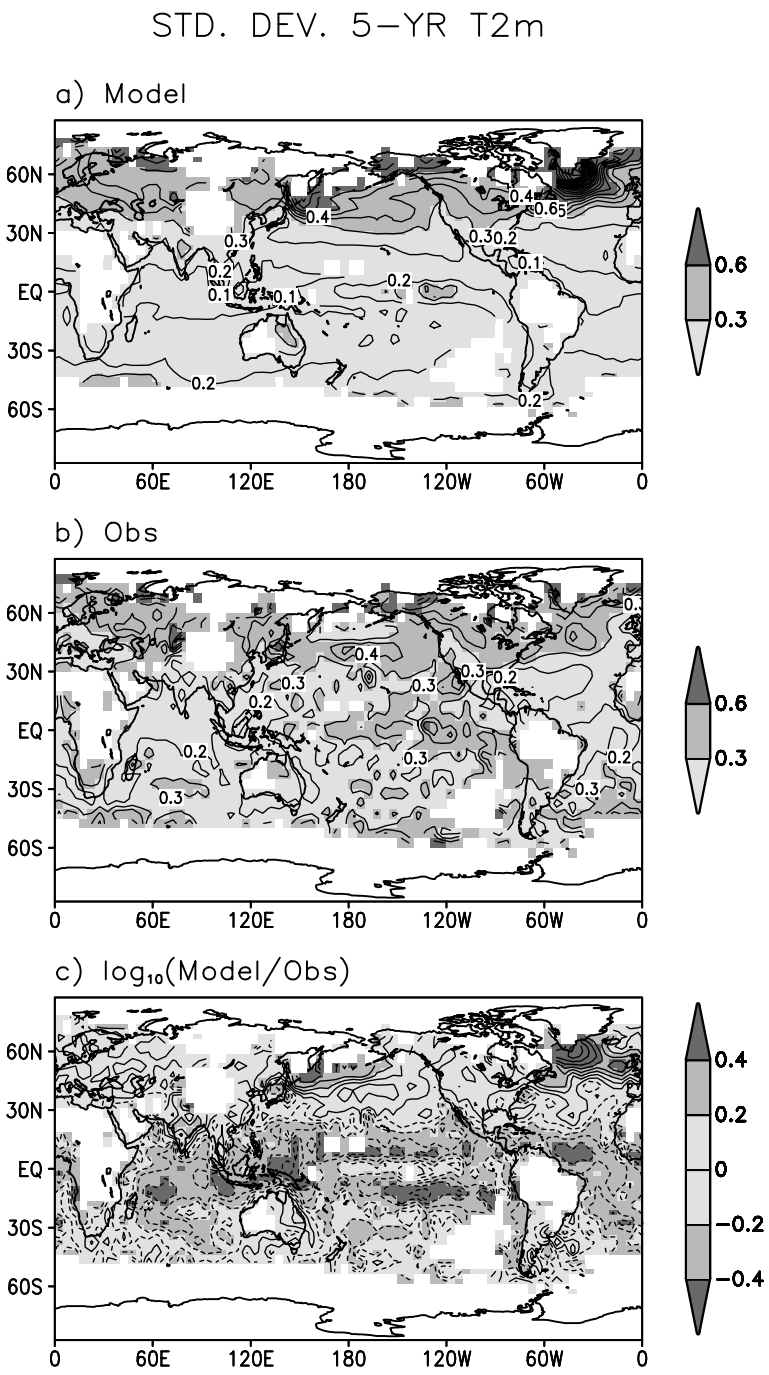

Fig. 7. Same as Fig. 6 but for 5-yr mean T2m. Contour intervals are 0.1°C in (a) and (b) and 0.1 in (c).

interannual STD are required to obtain non-missing observations. Figure 6 shows variability patterns of annual mean T2m. The observed pattern shows dominant variability (>1.0°C) on the continents north of 60°N and large variability (>0.5°C) in the NH mid-latitudes (Fig. 6b). Patches of large STD also occur over the North Pacific and the North Atlantic, as well as over the equatorial eastern Pacific (>0.5°C). Overall, the model captures the observed features of temperature variability quite well (Fig. 6a), but the logarithm of the ratio of model and observational variability (Fig. 6c) shows that the model has larger variability than observed in the North Pacific, North Atlantic and Himalayan Mountains, and smaller variability over the rest of the ocean, especially in the tropics. The decadal variability of surface temperatures computed from 5-yr mean time series (Fig. 7b) shows characteristics similar to those described above (more than 3-yr annual means are considered for non-missing 5-yr means).

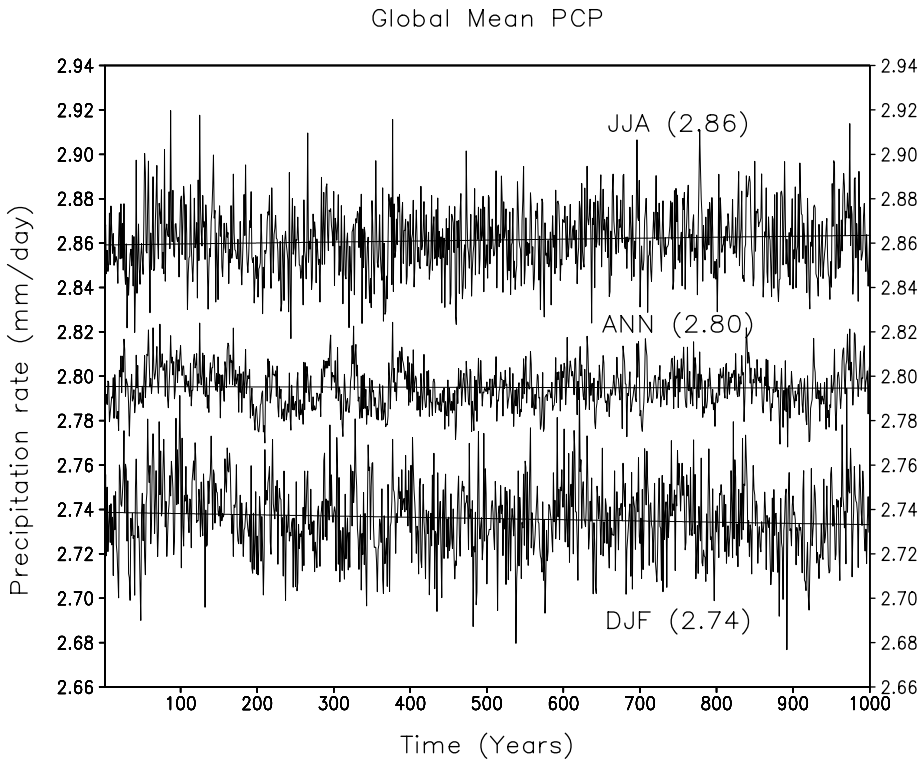

Fig. 8. Same as Fig. 1 but for PCP (mm d^{-1}). Observational values estimated from CMAP (1979–1998) are 2.68, 2.64 and 2.78 mm d^{-1} for ANN, DJF and JJA, respectively.

Larger variability is observed in high-latitude continents, the central North Pacific, North Atlantic and equatorial Pacific. The model simulates T2m variability over NH continents very well, but overestimates the variability in the North Pacific and North Atlantic, while the T2m variability in the tropical oceans is underestimated (Fig. 7c).

3.2. Precipitation

Figure 8 shows time series of ANN, DJF and JJA global mean PCP. As in the time series of T2m in Fig. 1, there is only little climate drift in the simulated PCP (-7.3×10^{-7} mm d^{-1} per century for ANN PCP). ECHO-G simulates a little more PCP than seen in the observations: climatological values of the global mean PCP rate in the model are 2.80, 2.74 and 2.86 mm d^{-1} for ANN, DJF and JJA mean, respectively. These values are 0.10–0.12 mm d^{-1} larger than observational values of 2.68, 2.64 and 2.78 mm d^{-1} estimated from the 20-yr mean (1979–1998) of CMAP data (Xie and Arkin, 1997). The amplitude of the model PCP seasonal cycle (JJA minus DJF) is 0.12 mm d^{-1} while the observed value is 0.14 mm d^{-1}.

A comparison of the simulated geographical distribution of DJF PCP with CMAP observations is shown in Fig. 9. The meridional distribution of zonal mean PCP is fairly well simulated by the model with a small wet bias over the NH mid-latitude and a dry bias near 40°S. The wet bias in the mid-latitude of the winter hemisphere is a common problem in CMIP AOGCMs (Lambert and Boer, 2001). The structure of the Intertropical Convergence Zone (ITCZ), the South Pacific Convergence Zone (SPCZ) and the dry tongue in the equatorial Pacific are well captured by the model, although the amplitudes of the ITCZ and SPCZ are slightly smaller than observed. Biases such as, for example, the positive deviations over South Africa, Australia and the western Indian Ocean are of the same order as those in ECHAM4 integrations with prescribed observed SST (Roeckner et al., 1996). The PCP in JJA is shown in Fig. 10. As in DJF, the overall pattern is well simulated by the model including the ITCZ and SPCZ structure. However, negative biases dominate in the Indian and Asian monsoon region and the eastern tropical Pacific. A maximum PCP appears over the Indian Ocean in the model, while it is positioned along the west coast of India and over the Bay of Bengal in the observations. This shortcoming also appeared in ECHAM4 stand-alone simulations (Roeckner et al., 1996), indicating that the monsoon simulation of the model is not affected by the coupling system applied here. In contrast to the DJF result, a wet bias is seen in JJA PCP over the Southern Hemisphere (SH) mid-latitudes. The zonal mean JJA PCP represents a good performance except for the wet bias in the SH mid-latitude.

The local temporal variability of annual mean PCP in the model is compared with 20-yr CMAP observations in Fig. 11.

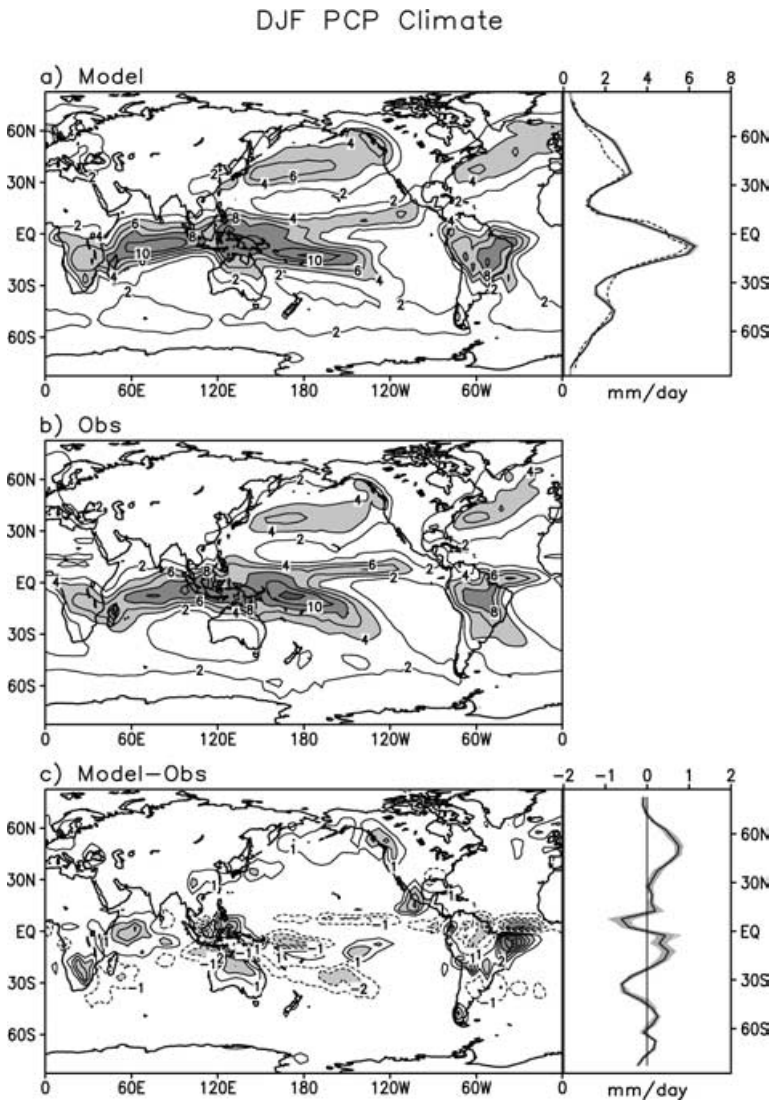

Fig. 9. PCP climate in DJF for model (a), observations (b), and model minus observation (c). Contour intervals are 2 mm d^{-1} in (a) and (b) and 1 mm d^{-1} in (c). Solid lines are for positive values, dotted lines for negative values, and the zero line is omitted in (c). Light solid lines in the zonal mean plots represent the results from 49 20-yr subsections of ECHO-G CTL.

The model STD is evaluated at each grid point by averaging 50 STDs calculated from 20-yr subperiods. As in the case of T2m variability in Figs. 6 and 7, the long-term linear trends are removed locally in advance for both simulations and observations. The observed pattern of interannual variability of precipitation (Fig. 11b) reveals dominant variability (>1.0 mm d^{-1}) in a zonal band of the tropical Pacific and eastern Indian Ocean with a maximum larger than 2 mm d^{-1} in the equatorial central Pacific. The meridional extent of larger variability (>0.5 mm d^{-1}) is from 30°S in the central Pacific to 30°N in the western Pacific. The equatorial Atlantic also shows larger variability. The overall pattern of the PCP variability is captured reasonably well by the model. However, its amplitude is lower than that observed in the eastern and western equatorial Pacific, South America, northwestern Pacific and equatorial western Africa. It is noted that the spatial pattern of the precipitation variability in the model and observations is dominated by ENSO-related fluctuations on the time-scale considered here. The decadal variability cannot be studied because of the short length of the observational period of 20 yr.

3.3. *Mean sea level pressure*

Figure 12 shows geographical and zonal mean patterns of DJF MSLP of ECHO-G CTL and observations (1961–1990 mean of NCEP/NCAR reanalysis; a different mean period, e.g. 1979–2003, does not change the result including biases in Antarctica – see below), as well as their differences. The comparison of zonal mean reveals overall good consistency between the model and observation, such as the tropical low, subtropical highs and high-latitude lows. The zonal mean pattern of the model bias reveals that the subtropical highs in the NH and the high-latitude lows have positive pressure biases. The amplitude of the model bias is less than 5 hPa except for the Southern Ocean and Antarctic

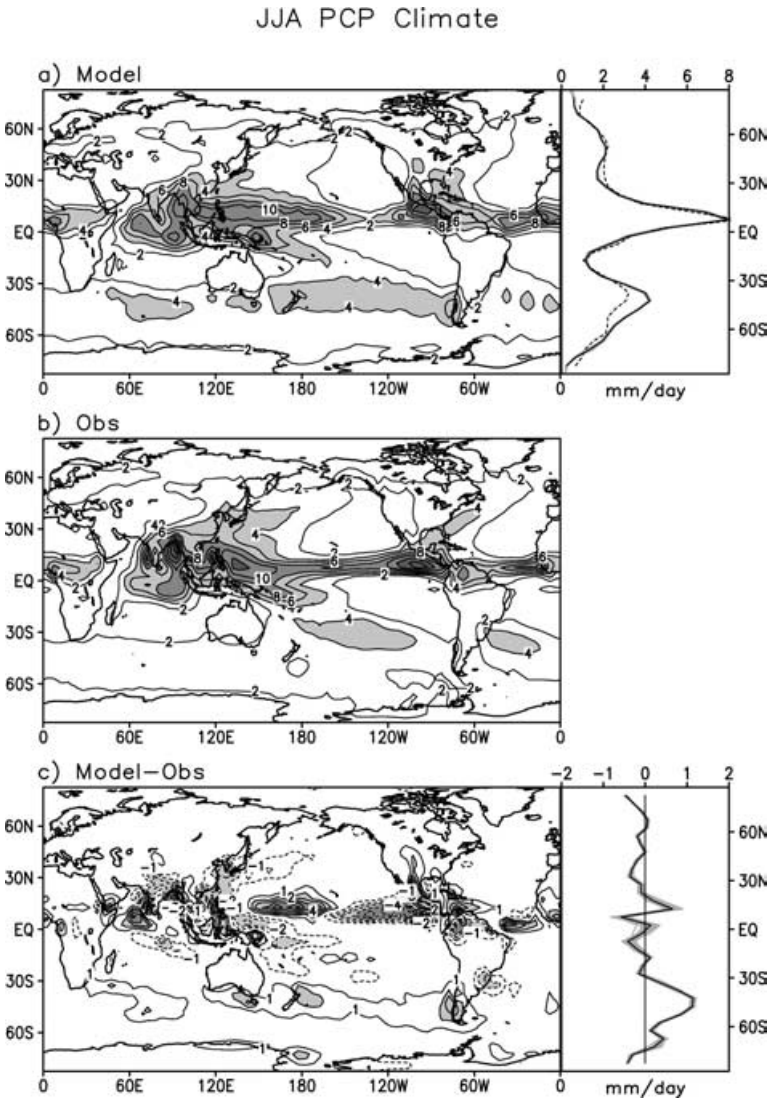

Fig. 10. Same as Fig. 9 but for JJA PCP (mm d^{-1}). Light solid lines in the zonal mean plots represent the results from 50 20-yr subsections of ECHO-G CTL.

regions. When compared with other AOGCMs, ECHO-G exhibits a relatively good skill in simulating the zonal mean MSLP, especially at the low and mid-latitudes (Lambert and Boer, 2001). The overall geographical patterns of the DJF mean MSLP are well represented in the model CTL including the position and amplitude of the main high- and low-pressure systems in the NH. The Aleutian Low and the Icelandic Low are well reproduced, except that the centre of the Aleutian Low is located more eastward in the model climate than in the observations. The Siberian High in the model is stronger especially in the northern part of Siberia. The Azores High in the model is stronger by more than 8 hPa and has a more eastward position. On the other hand, the subtropical highs in the SH mid-latitude have weak negative pressure biases while the Antarctic region has a strong positive bias. The positive bias over Antarctica may partly result from a lack of ozone depletion in the model (e.g. Thompson and Solomon, 2002; Gillett and Thompson, 2003). The stand-alone version of ECHAM4 shows very similar patterns of model bias in DJF MSLP (Roeckner et al., 1996), which indicates that the coupled system does not change significantly the climate of the atmospheric surface pressure, as is the case for PCP.

A comparison of JJA MSLP is shown in Fig. 13. The model climate captures the overall pattern of observations quite well, except for higher latitude regions in both hemispheres. The strong biases south of 60°S may be artefacts caused by large errors in the reanalysis MSLP in this region (Marshall and Harangozo, 2000; Marshall, 2003). The subtropical highs in the North Pacific and North Atlantic are simulated well both in position and strength. The Eurasian continental low in the model has a positive bias or weaker strength than observed, which may be related to the cold bias there and the weak summer monsoon (see above). The southern part of North America has a negative bias.

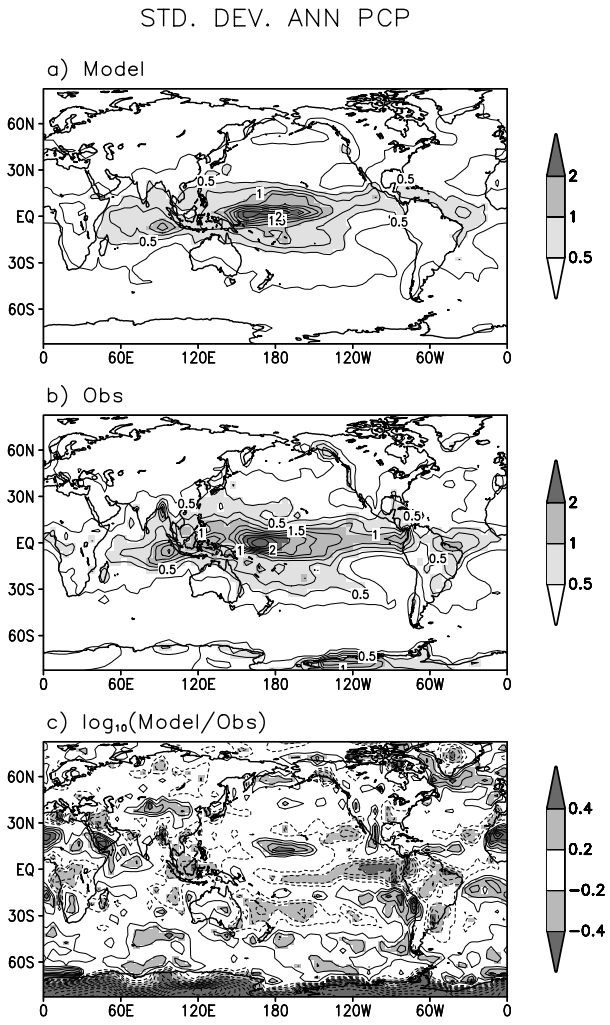

Fig. 11. Same as Fig. 6 but for precipitation. Contour intervals are 0.5 mm d^{-1} in (a) and (b) and 0.1 in (c). The zero line is omitted in (c).

Subtropical highs on the SH are well positioned, but they are slightly weaker than observed. A large negative bias appears in the SH mid-latitudes.

In order to assess the model skill in simulating the interannual variability, the STD of annual mean MSLP is calculated at each grid point and its horizontal distribution is shown in Fig. 14. The STD of the observed MSLP is evaluated from the 40-yr period (1961–2000) of NCEP/NCAR reanalysis while the STD of model climate is obtained by taking the mean of 25 STDs for 40-yr subsections of the 1000-yr CTL. The linear trends in the 40-yr period are removed for both model data and observations before calculating the STDs. The observed pattern of MSLP variability displays large variability (>1.5 hPa) in the North Pacific, North Atlantic and polar regions in both hemispheres. This appears to be related to the North Pacific Oscillation (NPO), NAO, Arctic Oscillation (AO) and Antarctic Oscillation (AAO) or hemispheric annular modes (Rogers, 1990; Thompson and Wallace, 1998, 2000, 2001); see also fig. 12 of Paper II for DJFM MSLP variability in the NH extratropics. It is also observed that generally the amplitude of MSLP variability is larger at higher latitude than at lower latitude, and over the oceans than over land. Figure 14 shows that ECHO-G is able to reproduce the overall pattern of the observed MSLP variability, but mostly with smaller amplitudes than observed. Exceptions are relatively large model variability over the equatorial central Pacific (>0.5 hPa), which might be related to the strong and regular El Niño-like variability in the model (see Paper II), and over the northern North Pacific. Other models might show different features of MSLP variability, e.g. less variability at high-latitude oceans than observed (Flato et al., 2000, for CGCM1).

4. Conclusions

In this paper we describe the climate and internal variability of a 1000-yr CTL with the coupled climate model ECHO-G using present constant values of well-mixed greenhouse gases and no external forcing. It provides a background for future scenario simulations. ECHO-G consists of the atmospheric component ECHAM4 and the oceanic component HOPE-G, and includes a dynamic and thermodynamic sea-ice model. Flux adjustments are applied for annual-mean heat and freshwater only, with zero global mean, and there is no adjustment in high latitudes poleward of the climatological AMIP ice edge. The model simulates almost no climate drift.

The internal variability of three surface variables (T2m, PCP and MSLP) are examined. The ECHO-G control experiment shows overall good skill in simulating the seasonal mean climatology and the interannual variability of T2m, PCP and MSLP. Biases in the model climate of the three variables are very similar to those of ECHAM4 stand-alone integrations (Roeckner et al., 1996) except for the JJA T2m in the Arctic region, which may be related to the partial sea-ice cover used in the coupled model in contrast to the stand-alone integrations (see Grötzner et al., 1996).

There appears a too strong 2-yr peak in the simulated global mean T2m power spectrum; accordingly the period of 3–9 yr has lower power than observed. This is closely related to the 2-yr regular period of the ENSO in the model (see Paper II for more details and discussion). Local temporal variability of the T2m at interannual to interdecadal time-scales is reproduced realistically over the NH continents, but it is overestimated over the North Pacific and North Atlantic while underestimated over the tropical oceans.

ECHO-G locates the ITCZ and SPCZ realistically, although there are biases in amplitudes. The PCP associated with the Indian and Asian summer monsoon is underestimated, which is speculated to be linked with the cold bias in the Asian continental T2m (i.e. weak land–sea temperature contrast) and with the weakly simulated Eurasian continental low in the model. The

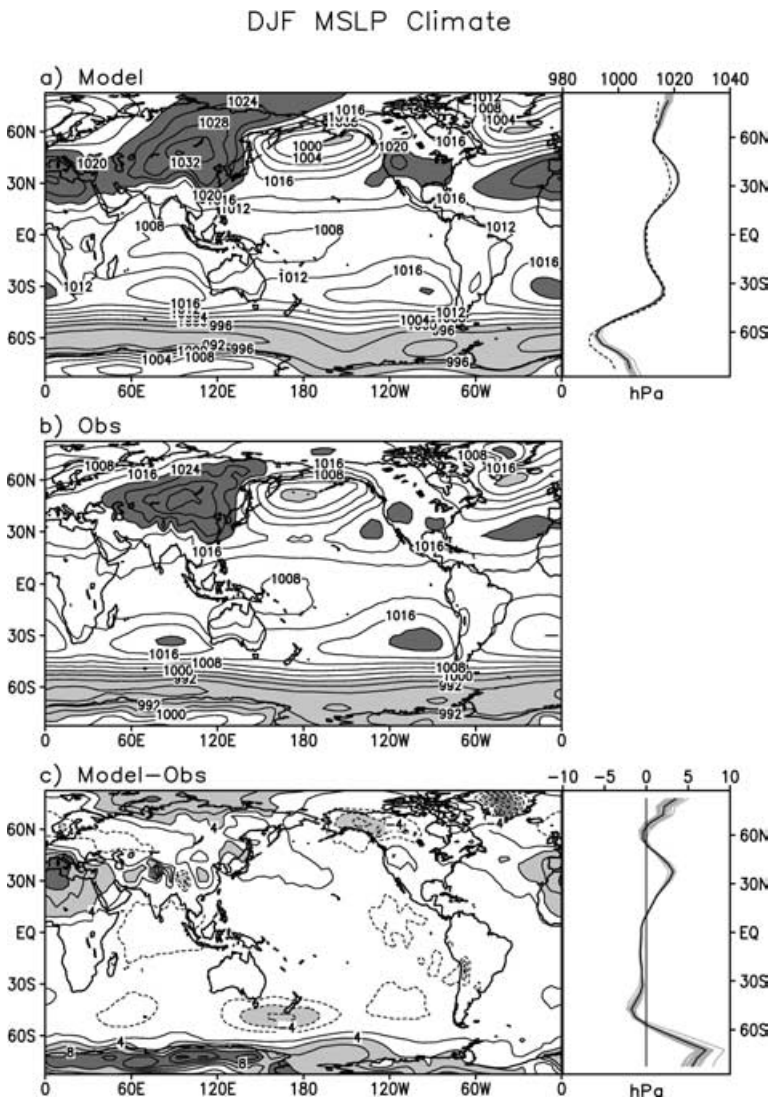

Fig. 12. MSLP climate in DJF for model (a), observations (b), and model minus observation (c). Contour intervals are 4 hPa in (a) and (b) and 2 hPa in (c). Solid lines are for positive values, dotted lines for negative values, and the zero line is omitted in (c). Light solid lines in the zonal mean plots represent the results from 33 30-yr subsections of ECHO-G CTL.

observed large variability of PCP in the tropical Pacific is well captured by the model but its amplitude is underestimated.

The spatial pattern of the MSLP STD exhibits weaker variability over Africa and the tropical western Pacific than the observations. The observed variability of the NH wintertime MSLP is characterized by two centres of action over the North Atlantic and the North Pacific. The pattern of MSLP variability in ECHO-G CTL shows locations and amplitudes similar to those observed.

A simple detection study of global mean T2m shows that the recent global positive 20–146 yr trends cannot be explained by the internal variability of ECHO-G CTL consistent with previous studies with other models (e.g. Collins et al., 2001, for HadCM3).

5. Acknowledgments

This research was performed for the project 'Research on the Development of Regional Climatic Change Scenarios to Prepare the National Climate Change Report' of the Korean Meteorological Research Institute and for the DFG (German Research Foundation) project He1916/8. The model was run on a NEC SX-4 at the DKRZ, Hamburg, Germany.

References

Baquero-Bernal, A., Latif, M. and Legutke, S. 2002. On dipole-like variability of sea surface temperature in the tropical Indian Ocean. *J. Climate* **15**, 1358–1368.

Barnett, T. P., Hasselmann, K., Chelliah, M., Delworth, T., Hegerl, G. and co-authors. 1999. Detection and attribution of recent climate change: a status report. *Bull. Am. Meteorol. Soc.* **80**, 2631–2659.

Blackman, R. B. and Tukey, J. W. 1958. *The Measurement of Power Spectra From the Point of View of Communication Engineering*, Dover Publications, New York, 190 pp.

Braganza, K., Karoly, D. J., Hirst, A. C., Mann, M. E., Stott, P. and co-authors. 2002. Simple indices of global climate variability and

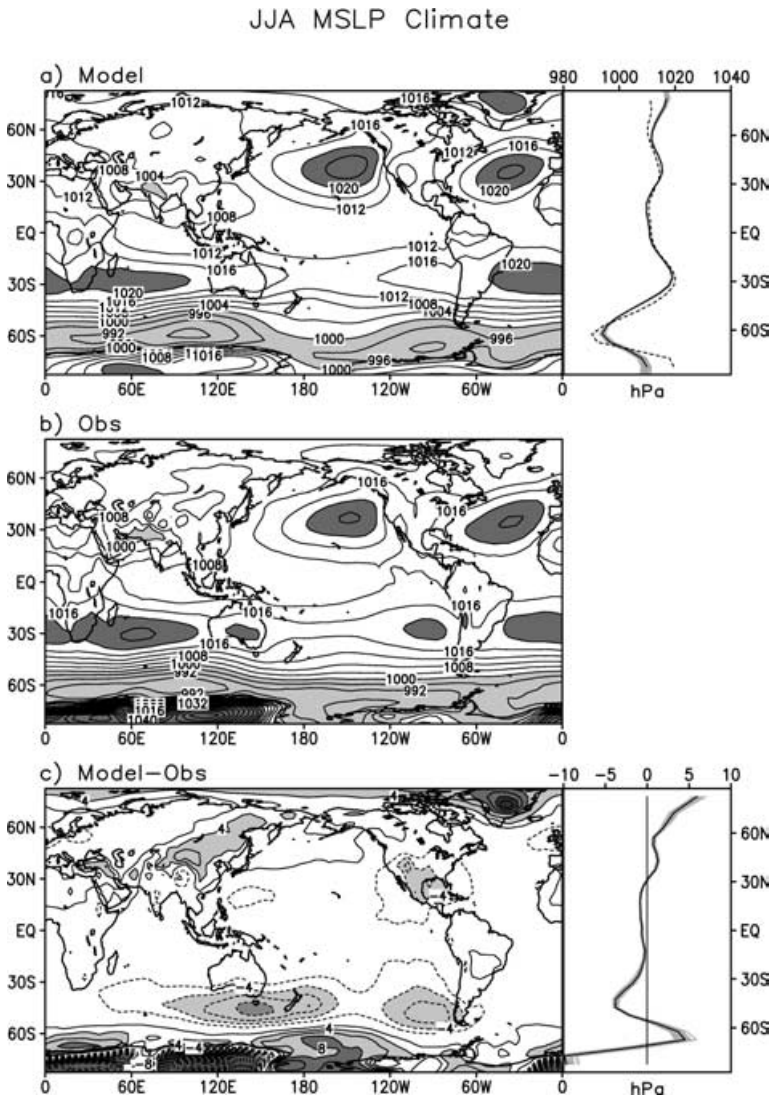

Fig. 13. Same as Fig. 12 but for JJA MSLP.

change: Part I – variability and correlation structure. *Climate Dyn.* **20**, 491–502.

Collins, M. 2000. The El-Niño Southern Oscillation in the second Hadley Centre coupled model and its response to greenhouse warming. *J. Climate* **13**, 1299–1312.

Collins, M., Tett, S. F. B. and Cooper, C. 2001. The internal climate variability of HadCM3, a version of the Hadley Centre coupled model without flux adjustments. *Climate Dyn.* **17**, 61–81.

Delworth, T. L., Stouffer, R. J., Dixon, K. W., Spelman, M. J., Knutson, T. R. and co-authors. 2002. Review of simulations of climate variability and change with the GFDL R30 coupled climate model. *Climate Dyn.* **19**, 555–574.

Flato, G. M., Boer, G. J., Lee, W. G., McFarlane, N. A., Ramsden, D. and co-authors. 2000. The Canadian Centre for Climate Modelling and Analysis global coupled model and its climate. *Climate Dyn.* **26**, 451–467.

Frey, H., Latif, M. and Stockdale, T. 1997. The coupled GCM ECHO-2. Part I: The tropical Pacific. *Mon. Wea. Rev.* **125**, 703–720.

Gillett, N. P., Allen, M. R. and Tett, S. F. B. 2000. Modelled and observed variability in atmospheric vertical temperature structure. *Climate Dyn.* **16**, 49–61.

Gillett, N. P. and Thompson, D. W. J. 2003. Simulation of recent Southern Hemisphere climate change. *Science* **302**, 273–275.

Grötzner, A., Sausen, R. and Claussen, M. 1996. The impact of sub-grid scale sea-ice inhomogeneities on the performance of the atmospheric general circulation model ECHAM3. *Climate Dyn.* **12**, 477–496.

Grötzner, A., Latif, M. and Barnett, T. P. 1998. A decadal climate cycle in the North Atlantic Ocean as simulated by the ECHO coupled GCM. *J. Climate* **11**, 831–847.

Hasselmann, K. 1976. Stochastic climate models. Part 1: Theory. *Tellus* **28A**, 473–485.

Hibler, W. D. III. 1979. A dynamic thermodynamic sea-ice model. *J. Phys. Oceanogr.* **9**, 817–846.

Hirst, A. C., O'Farrell, S. P. and Gordon, H. B. 2000. Comparison of a coupled ocean–atmosphere model with and without oceanic

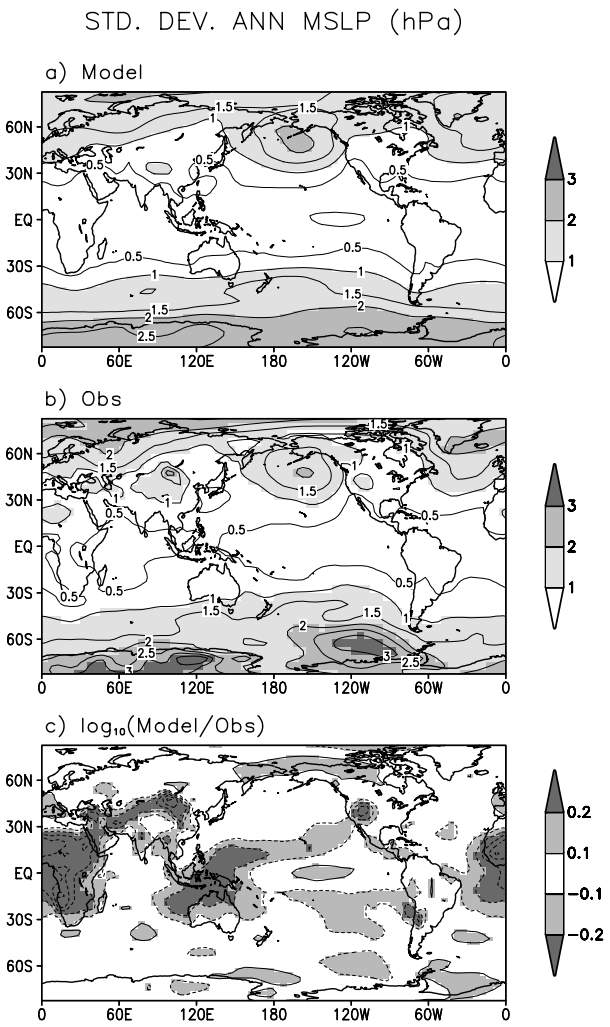

Fig. 14. Same as Fig. 6 but for the MSLP. Contour intervals are 0.5 hPa in (a) and (b) and 0.1 in (c). The zero line is omitted in (c).

eddy-induced advection. Part I: Ocean spin-up and control integrations. *J. Climate* **13**, 139–163.

Holland, M. M. 2003. The North Atlantic Oscillation–Arctic Oscillation in the CCSM2 and its influence on Arctic climate variability. *J. Climate* **16**, 2767–2781.

Hu, Z. Z., Latif, M., Roeckner, E. and Bengtsson, L. 2000. Intensified Asian summer monsoon and its variability in a coupled model forced by increasing greenhouse gas concentrations. *Geophys. Res. Lett.* **27**, 2681–2684.

Hu, A., Meehl, G. A. and Han, W. 2004. Detecting thermohaline circulation changes from ocean properties in a coupled model. *Geophys. Res. Lett.* **31**, (doi:10.1029/2004GL020218).

Hunt, B. G. and Elliott, T. I. 2003. Secular variability of ENSO events in a 1000-yr climate simulation. *Climate Dyn.* **20**, 689–703.

Jones, P. D. and Moberg, A. 2003. Hemispheric and large-scale surface air temperature variations: an extensive revision and an update to 2001. *J. Climate* **16**, 206–223.

Jones, P. D., New, M., Parker, D. E., Martin, S. and Rigor, I. G. 1999. Surface air temperature and its changes over the past 150 yr. *Rev. Geophys.* **37**, 173–199.

Kiehl, J. T. and Gent, P. R. 2004. The Community Climate System Model, version 2. *J. Climate* **17**, 3666–3682.

Kistler, R., Kalnay, E., Collins, W., Saha, S., White, G. and co-authors. 2001. The NCEP/NCAR 50-yr reanalysis: monthly means CD-ROM and documentation. *Bull. Am. Meteorol. Soc.* **82**, 247–267.

Lambert, S. J. and Boer, G. J. 2001. CMIP1 evaluation and intercomparison of coupled climate models. *Climate Dyn.* **17**, 83–106.

Latif, M. and Barnett, T. P. 1994. Causes of decadal climate variability over the North Pacific and North Atlantic. *Science* **266**, 634–637.

Latif, M. and Barnett, T. P. 1996. Decadal climate variability over the North Pacific and North America: dynamics and predictability. *J. Climate* **9**, 2407–2423.

Latif, M., Stockdale, T., Wolff, J.-O., Burgers, G., Maier-Reimer, E. and co-authors. 1994. Climatology and variability in the ECHO coupled GCM. *Tellus* **46A**, 351–366.

Legutke, S. 2000. Sea ice in coupled climate models: impact of high-latitude freshwater fluxes. *WCRP informal report No. 6*, 25–28.

Legutke, S. and Maier-Reimer, E. 1999. Climatology of the HOPE-G global ocean general circulation model. *Technical report No. 21*, German Climate Computer Centre (DKRZ), Hamburg, Germany, 90 pp.

Legutke, S. and Voss, R. 1999. The Hamburg atmosphere–ocean coupled circulation model ECHO-G. *Technical report No. 18*, German Climate Computer Centre (DKRZ), Hamburg, Germany, 62 pp.

Legutke, S., Maier-Reimer, E., Cubasch, U. and Hellbach, A. 1996. Sensitivity of an OGCM to the resolution of atmospheric forcing data. In: *CAS/JSC Working Group Numerical Experimentation, Report No. 20* (ed. G. J. Boer). World Climate Research Program, WMO.

Manabe, S. and Stouffer, R. J. 1996. Low-frequency variability of surface air temperature in a 1000-yr integrations of a coupled atmosphere–ocean–land surface model. *J. Climate* **9**, 376–393.

Marshall, G. J. 2003. Trends in the Southern Annular Mode from observations and reanalyses. *J. Climate* **16**, 4134–4143.

Marshall, G. J. and Harangozo, S. A. 2000. An appraisal of NCEP/NCAR reanalysis MSLP data viability for climate studies in the South Pacific. *Geophys. Res. Lett.* **27**, 3957–3060.

Marsland, S. J., Latif, M. and Legutke, S. 2003. Antarctic circumpolar modes in a coupled ocean–atmosphere model. *Ocean Dyn.* **53**, 323–331.

Min, S.-K., Legutke, S., Hense, A. and Kwon, W.-T. 2005. Internal variability in a 1000-yr control simulation with the coupled climate model ECHO-G – II. El Niño Southern Oscillation and North Atlantic Oscillation. *Tellus* **57A**, 622–640.

Monahan, A. H. and Dai, A. 2004. The spatial and temporal structure of ENSO non-linearity. *J. Climate* **17**, 3026–3036.

Osborn, T. J., Briffa, K. R., Tett, S. F. B., Jones, P. D. and Trigo, R. M. 1999. Evaluation of the North Atlantic Oscillation as simulated by a coupled climate model. *Climate Dyn.* **15**, 685–702.

Pierce, D. W., Barnett, T. P. and Latif, M. 2000. Connections between the Pacific Ocean tropics and mid-latitudes on decadal time-scales. *J. Climate* **13**, 1173–1194.

Rayner, N. A., Horton, E. B., Parker, D. E., Folland, C. K. and Hackett, R. B. 1996. Version 2.2 of the global sea-ice and sea surface temperature data set, 1903–1994. *Hadley Centre Climate Research Techn*

Note, CRTN 74, September, Hadley Centre, Meteorological Office, Bracknell, UK, 21 pp.

Rayner, N. A., Parker, D. E., Horton, E. B., Folland, C. K., Alexander, L. V. and co-authors. 2003. Global analyses of SST, sea ice and night marine air temperature since the late nineteenth century. *J. Geophys. Res.* **108**(D14), 4407 (doi:10.1029/2002JD002670).

Rodgers, K. B., Friederichs, P. and Latif, M. 2004. Tropical Pacific decadal variability and its relation to decadal modulations of ENSO. *J. Climate* **17**, 3761–3774.

Roeckner, E., Arpe, K., Bengtsson, L., Christoph, M., Claussen, M. and co-authors. 1996. The atmospheric general circulation model ECHAM-4: model description and simulation of present-day climate. *Report No. 218*, Max Planck Institute for Meteorology, Hamburg, Germany, 90 pp.

Rogers, J. C. 1990. Patterns of low-frequency monthly sea level pressure variability (1899–1986) and associated wave cyclone frequencies. *J. Climate* **3**, 1364–1379.

Schneider, N., Barnett, T., Latif, M. and Stockdale, T. 1996. Warm pool physics in a coupled GCM. *J. Climate* **9**, 219–239.

Stendel, M. and Roeckner, E. 1998. Impacts of horizontal resolution on simulated climate statistics in ECHAM4. *Report No. 253*, Max Planck Institute for Meteorology, 57 pp.

Stouffer, R. J., Hegerl, G. and Tett, S. 2000. A comparison of surface air temperature variability in three 1000-yr coupled ocean–atmosphere model integrations. *J. Climate* **13**, 513–537.

Tett, S. F. B., Johns, T. C. and Mitchell, J. F. B. 1997. Global and regional variability in a coupled AOGCM. *Climate Dyn.* **13**, 303–323.

Thompson, D. W. J. and Solomon, S. 2002. Interpretation of recent Southern Hemisphere climate change. *Science* **296**, 895–899.

Thompson, D. W. J. and Wallace, J. M. 1998. The Arctic Oscillation signature in the wintertime geopotential height and temperature fields. *Geophys. Res. Lett.* **25**, 1297–1300.

Thompson, D. W. J. and Wallace, J. M. 2000. Annular modes in the extratropical circulation. Part I: Month-to-month variability. *J. Climate* **13**, 1000–1016.

Thompson, D. W. J. and Wallace, J. M. 2001. Regional climate impacts of the Northern Hemisphere Annular Mode. *Science* **293**, 85–89.

Timmermann, M., Latif, A., Grötzner, A. and Voss, R. 1999. Modes of climate variability as simulated by a coupled general circulation model. Part I: ENSO-like variability and its low-frequency modulation. *Climate Dyn.* **15**, 605–618.

Valcke, S., Terray, L. and Piacentini, A. 2000. The OASIS Coupler User Guide, Version 2.4. *Technical report TR/CMGC/00–10*, CERFACS, 77 pp.

Venzke, S., Latif, M. and Villwock, A. 2000. The coupled GCM ECHO-2. Part II: Indian Ocean response to ENSO. *J. Climate* **13**, 1371–1383.

Vimont, D. J., Battisti, D. S. and Hirst, A. C. 2002. Pacific interannual and interdecadal equatorial variability in a 1000-yr simulation of the CSIRO coupled general circulation model. *J. Climate* **15**, 160–178.

von Storch, J. S., Kharin, V. V., Cubasch, U., Hegerl, G. C., Schriever, D. and co-authors. 1997. A description of a 1260-yr control integration with the coupled ECHAM1/LSG general circulation model. *J. Climate* **10**, 1525–1543.

von Storch, J. S., Müller, P., Stouffer, R. J., Voss, R. and Tett, S. F. B. 2000. Variability of deep-ocean mass transport: spectral shapes and spatial scales. *J. Climate* **13**, 1916–1935.

von Storch, J. S., Müller, P. and Bauer, E. 2001. Climate variability in millennium integrations with coupled atmosphere–ocean GCMs: a spectral view. *Climate Dyn.* **17**, 375–389.

Voss, R., Sausen, R. and Cubasch, U. 1998. Periodically synchronously coupled integrations with the atmosphere–ocean general circulation model ECHAM3/LSG. *Climate Dyn.* **14**, 249–266.

Washington, W. M., Weatherald, J. W., Meehl, G. A., Semtner, A. J. Jr, Bettge, T. W. and co-authors. 2000. Parallel climate model (PCM) control and transient simulations. *Climate Dyn.* **16**, 755–774.

Wolff, J.-O., Maier-Reimer, E. and Legutke, S. 1997. The Hamburg Ocean Primitive Equation Model. *Technical report No. 13*, German Climate Computer Center (DKRZ), Hamburg, Germany, 98 pp.

Xie, P. and Arkin, P. A. 1997. Global precipitation: a 17-yr monthly analysis based on gauge observations, satellite estimates, and numerical model outputs. *Bull. Am. Meteorol. Soc.* **78**, 2539–2558.

Yu, B. and Boer, G. J. 2004. The role of the western Pacific in decadal variability. *Geophys. Res. Lett.* **31**, doi:10.1029/2003GL018471.

Zorita, E., González-Rouco, F. and Legutke, S. 2003. Testing the Mann et al. (1998) approach to paleoclimate reconstructions in the context of a 1000-yr control simulation with the ECHO-G coupled climate model. *J. Climate* **16**, 1378–1390.